Intermittency-induced criticality in a resistor-inductor-diode circuit

Stelios M. Potirakis,[1,*] Yiannis Contoyiannis,[1,†] Fotios K. Diakonos,[2,‡] and Michael P. Hanias[2,§]
[1]*Department of Electronics Engineering, Piraeus University of Applied Sciences (TEI Piraeus), 250 Thivon and P. Ralli, Aigaleo, Athens GR-12244, Greece*
[2]*Department of Physics, University of Athens, GR-15771 Athens, Greece*
(Received 31 October 2016; revised manuscript received 13 March 2017; published 12 April 2017)

The current fluctuations of a driven resistor-inductor-diode circuit are investigated here looking for signatures of critical behavior monitored by the driving frequency. The experimentally obtained time series of the voltage drop across the resistor (as directly proportional to the current flowing through the circuit) were analyzed by means of the method of critical fluctuations in analogy to thermal critical systems. Intermittent criticality was revealed for a critical frequency band signifying the transition between the normal rectifier phase in the low frequencies and a full-wave conducting, capacitorlike phase in the high frequencies. The transition possesses critical characteristics with a characteristic exponent $p_l = 1.65$. A fractal analysis in terms of the rescale range (R/S) and detrended fluctuation analysis methods yielded results fully compatible with the critical dynamics analysis. Suggestions for the interpretation of the observed behavior in terms of p-n junction operation are discussed.

DOI: 10.1103/PhysRevE.95.042206

I. INTRODUCTION

The dynamics of nonautonomous, sinusoidally driven, resistor-inductor-diode (RLD) series circuits has extensively been studied in the literature, for a variety of diode types. Different scenarios which may lead to chaotic behavior have been explored and different models explaining the observed nonlinear evolution have been proposed, e.g., [1–17]. Most of the studies focus on the behavior at high driving frequencies, around the resonant frequency of the circuit.

A basic dynamical mechanism leading to chaotic behavior in electronic circuits is intermittency. Several forms of maps have been proposed to describe the associated intermittent dynamics. Among others, Rollins and Hunt [5,8], studying a serial diode resonator circuit, proposed a one-dimensional monoparametric mapping function describing the evolution of the maximum forward current through the diode. The authors associated the appearance of intermittency in this map with the onset of a crisis phenomenon when the driving voltage amplitude exceeds a critical value. Moreover, Jeffries and Perez [4] studied experimentally the same circuit with the voltage amplitude as control parameter. From the equations of the circuit, they deduced a logistic map which shows intermittency type I at the first period 5 window [4]. de S. Cavalcante and Rios Leite [13] experimentally found evidence of a type-III intermittency of cubic nonlinearity in a driven RLD circuit. Moreover, intermittency has also been found in more complex circuits, for example, type III in an autonomous electronic circuit with negative resistance [18] and type II in coupled electronic nonlinear devices [19]. The derived maps demonstrated universal characteristics. This universality is expressed through the exponent ν determining the power-law distribution of the mean waiting time (or mean "laminar length"):

$$\langle l \rangle \sim \sigma^{-\nu}, \tag{1}$$

where σ is the distance of the voltage amplitude from the critical value: $\sigma = |V - V_c|$. We note that the term "waiting time" here denotes the number of successive time steps for which a trajectory remains within a predefined region around a marginally unstable fixed point.

For the electronic circuits mentioned above the value of ν has been found to be $\nu = 0.5$ [4,8]. This exponent is related to the exponent z in the normal form of the underlying intermittent map [20]; the value $\nu = 0.5$ corresponds to $z = 2$. Up to now, all the descriptions of the nonlinear phenomena appearing in the p-n junction are based on concepts of chaotic dynamics such as period doubling, bifurcations, intermittency, etc., characterizing in particular the point of transition between the regular and chaotic behavior as crisis [4].

In this work, we attempt to describe the p-n junction operation in terms of concepts used in thermal critical phenomena. Specifically, we attempt to associate the intermittent dynamical behavior occurring in electronic circuits with the dynamics of the fluctuations of an order parameter in analogy to thermal critical systems, using the method of critical fluctuations (MCF) introduced in [21–24]. For this purpose, we investigate the evolution of the fluctuations of the voltage V_R across the resistor or equivalently the current I flowing through circuit components, in a driven RLD circuit, using the driving frequency as a control parameter. Our analysis shows that there is a critical transition zone of frequencies where the nonlinear properties of the circuit change, leading to a transition from the normal rectifier operation in the low frequencies to a full-wave conducting, capacitorlike operation in the high frequencies. This zone is characterized by the appearance of fluctuations in V_R (or I) which present intermittent behavior, similar to the dynamics of the order parameter fluctuations in a thermal critical system as in [22].

*Corresponding author: Department of Electronics Engineering, Piraeus University of Applied Sciences (TEI of Piraeus), 250 Thivon & P. Ralli, GR-12244 Aigaleo–Athens, Greece; spoti@puas.gr
†yconto@yahoo.gr
‡fdiakono@phys.uoa.gr
§mhanias@gmail.com

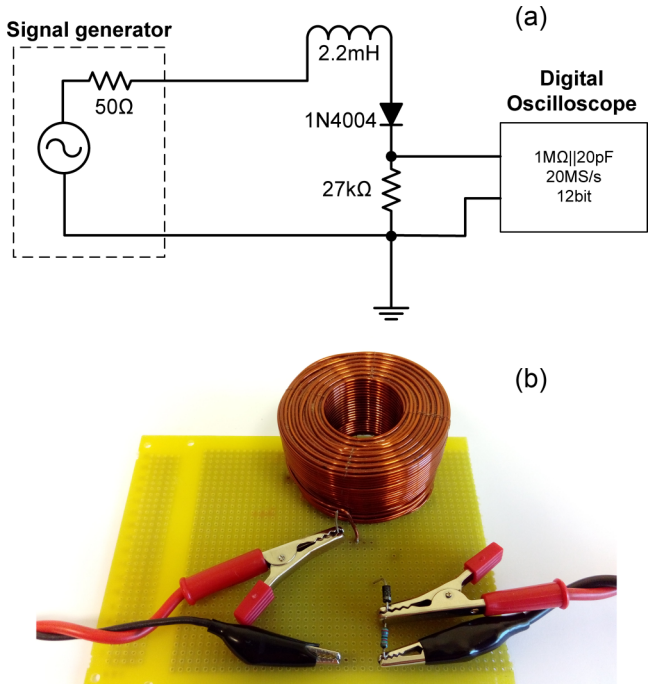

FIG. 1. (a) Experimental setup; values of the RLD circuit components and details about the used instruments are also shown. (b) Photograph of the circuit implementation used for experimentation.

The remainder of the article is organized as follows: Sec. II presents the employed RLD circuit and details about the conducted experiment; Sec. III sets a framework for the study of the RLD circuit in terms of MCF; the RLD circuit time series are analyzed using the MCF in Sec. IV; a complementary fractal analysis is performed in Sec. V; and finally, the main findings are discussed and conclusions are summarized in Sec. VI.

II. EXPERIMENTAL SETUP

The experimental setup and details of the employed circuit are shown in Fig. 1. The nonlinear element was a typical rectifier diode, 1N4004, while an air wound inductor of 2.2 mH inductance was used in order to exclude any inductor-core-induced nonlinearities from the experiment. Since we are interested in studying the diode current of a driven RLD circuit, we used a signal (waveform) generator having a 50-Ω output impedance to feed a sinusoidal driving signal to the circuit while acquiring the voltage drop $V_R(t)$ across the 27-kΩ resistor (as directly proportional to the circuit's current) by means of a digital oscilloscope of 12 bit resolution at a sampling rate of 20 MS/s. Conducting the experiment for different values of the driving signal frequency, one time series comprising at least 100 periods of $V_R(t)$ was acquired for each driving frequency. Note that during all experiments the same instruments were used [cf. Fig. 1(a) for their key characteristics], while the electromotive force of the signal generator was a sinus of peak value $V_o = 14$ V.

Figure 2 portrays typical examples of the three kinds of waveforms which were acquired during the aforementioned experiments. The waveform of Fig. 2(a) is part of the $V_R(t)$ time series for driving frequency $f = 1$ kHz and represents the behavior of diode current of the RLD circuit at low frequencies, a typical rectifying operation during which there are no negative $V_R(t)$ values. As driving frequency increases, negative undershoots appear [e.g., Fig. 2(b) for driving frequency $f = 5$ kHz] until there is complete loss of rectification in very high frequencies [e.g., Fig. 3(c) for driving frequency $f = 500$ kHz]. In the next section we proceed to the study of the rectifying phase (at low frequencies), the nonrectifying phase (at very high frequencies), and especially the transition between them.

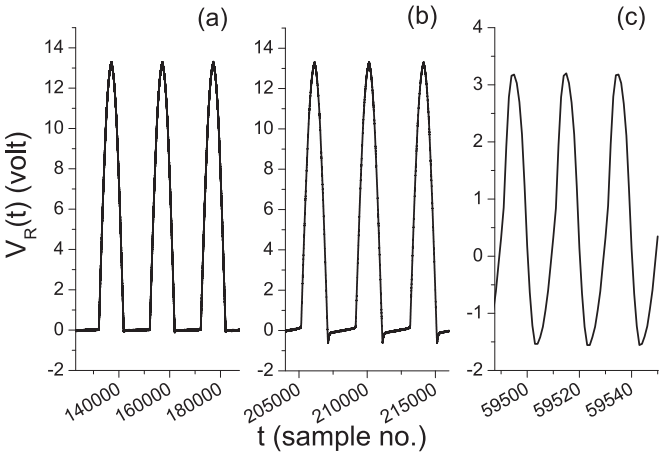

FIG. 2. The three kinds of acquired $V_R(t)$ waveforms. (a) Part of the 1 kHz time series as an example of the low-frequency rectifying behavior. (b) Part of the 5 kHz time series presenting undershoots entering the negative values region. (c) Part of the 500 kHz time series in the full-wave conducting, capacitorlike operation.

III. THE RECTIFYING-NONRECTIFYING PHASE TRANSITION IN THE RLD CIRCUIT

From the measurements obtained during our experiments (cf. Sec. II, Fig. 2), two discrete phases can be identified in

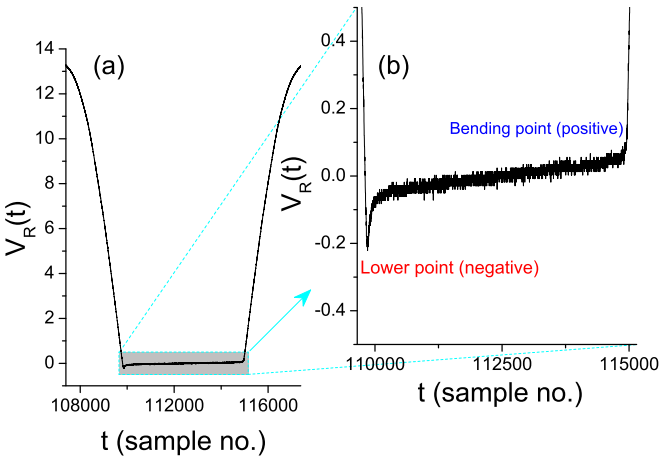

FIG. 3. (a) One full, arbitrarily selected period of the measured 2 kHz $V_R(t)$ time series. (b) Closeup of the lowest fluctuations of the 2 kHz $V_R(t)$ time series excerpt depicted in (a). The existence of reverse-recovery phenomenon is obvious.

p-n junction dynamics: (a) the rectifying phase (phase A) at the lower frequencies ($f < 1$ kHz) which is characterized by a typical diode behavior (acting as a rectifier) attributed to the one-way (half-wave) conduction character of the p-n junction, and (b) the nonrectifying phase (phase B) in very high frequencies ($f > 500$ kHz) where the diode conducts during the whole cycle of the driving signal having lost its rectifying properties and becoming a full-wave conducting, capacitorlike circuit element. A first observation is that a wide transition zone in the frequency space separates these two discrete phases.

This transition from phase A to phase B is connected with the so-called reverse-recovery time τ_{RR}. When the diode current is passing through zero, the diode does not shut off immediately, but continues to conduct for a time interval equal to τ_{RR}. This defines a characteristic time scale which has been intensively studied in the literature, e.g., [5,8,14]. In [14] the authors have investigated the appearance of chaotic behavior in circuit current for a wide range of frequencies and they have shown the existence of specific zones of the driving frequency where period doubling bifurcations take place.

At this point we need to focus on the phenomenon of interest, which is the transition from phase A to phase B. For this reason we consider the measured $V_R(t)$ time series at $f = 2$ kHz (an intermediate frequency between 1 and 500 kHz). In Fig. 3(a), one full, arbitrarily selected period of the specific time series is depicted, while a closeup of its lower part is shown in Fig. 3(b). The reverse-recovery time phenomenon make its appearance, indicated by the obvious voltage undershoot followed by a mild slope (slow) recovery. We focus our analysis in the lowest part of the $V_R(t)$ time series, around zero values.

The basic reason calling for such an approach is that we want to reveal the dynamics which are related with the appearance of the reverse-recovery time phenomenon in the lower part of the time series. Therefore, from the originally measured time series for each driving frequency we produce a time series comprising only the $V_R(t)$ values which fluctuate between the lower (negative) point and the (positive) bending point, as shown in Fig. 3(b). This time series will be designated as $V_{bt}(t)$. As an example, Fig. 4 depicts an arbitrary one-period-long excerpt of $V_{bt}(t)$ for $f = 5$ kHz. The time series, $V_{bt}(t)$, will be further analyzed as a candidate for presenting critical fluctuations. The main objective is to investigate whether there is any nontrivial dynamics in what, by a simple visual inspection, appears to be noise.

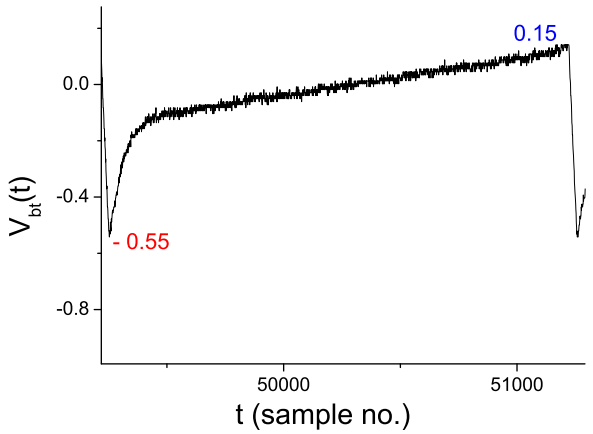

FIG. 4. The time series $V_{bt}(t)$ for $f = 5$ kHz has values in the region from -0.55 to 0.15 mV.

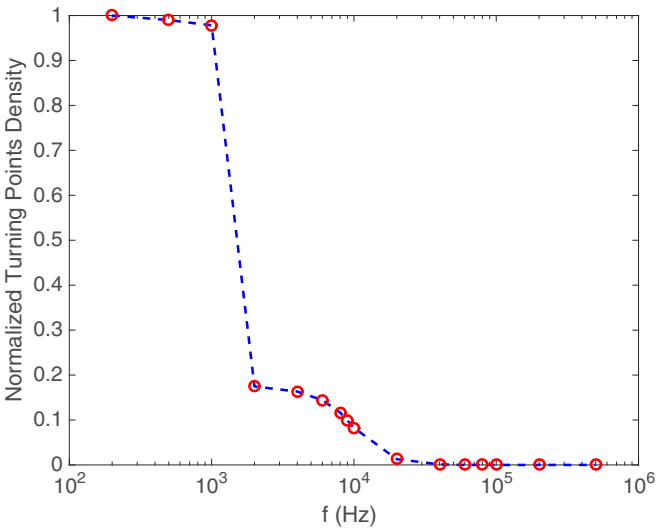

FIG. 5. Normalized density of turning points for different driving frequencies.

In a first attempt to check whether $V_{bt}(t)$ is an appropriate time series for our purposes, we estimated the density of turning points (local minima and maxima) in the $V_{bt}(t)$ time series obtained for different driving frequencies, as a measure of the presence of fluctuations. The turning points density was estimated as $\frac{\text{number of turning points}}{\text{length of the corresponding time series}}$. Figure 5 shows the normalized turning points density for different driving frequencies, clearly indicating the existence of three distinct frequency bands: (a) frequencies lower than $\sim$1 kHz, (b) from $\sim$2 kHz up to $\sim$10 kHz, and (c) frequencies higher than $\sim$20 kHz. This picture is in agreement with the aforementioned notions of phase A (band a), phase B (band c), and the transition from phase A to phase B (band b). Therefore, we consider that the study of the fluctuations in $V_{bt}(t)$ is a reasonable strategy for the investigation of the reverse-recovery time phenomenon and the dynamics associated with the transition from phase A to phase B. In the next section, Sec. IV, we proceed to the analysis of $V_{bt}(t)$ fluctuations using MCF. Note that the main advantage of MCF is exactly the ability to reveal dynamics "hidden" in intense noise [25]; therefore it is considered appropriate for studying the $V_{bt}(t)$ fluctuations.

IV. MCF ANALYSIS OF THE $V_{bt}(t)$ TIME SERIES

This method of critical fluctuations (MCF) has been extensively described in a series of works [21–24] and for this reason we avoid repeating it here. However, we will demonstrate step by step the application of MCF analysis for one of the analyzed time series [the $V_{bt}(t)$ for $f = 5$ kHz] for clarity reasons.

An excerpt of the analyzed 5 kHz $V_{bt}(t)$ time series is shown in Fig. 6(a). First, we check that it satisfies certain stationarity criteria (saturation of cumulative mean value and standard

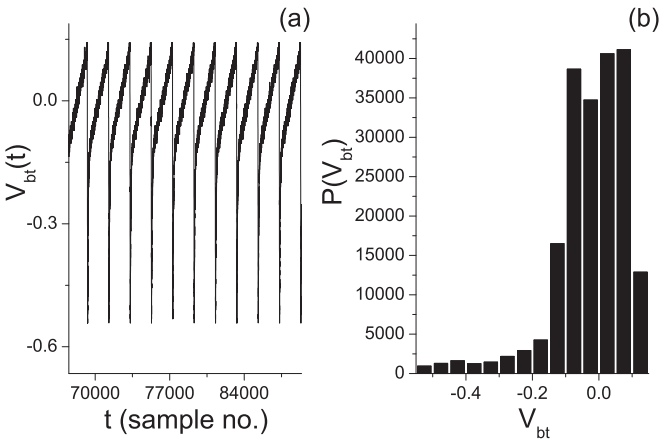

FIG. 6. (a) The time series $V_{bt}(t)$ for $f = 5$ kHz, resulting from the original time series $V_R(t)$ after the exclusion of the positive values above the bending point. (b) The distribution of the $V_{bt}(t)$ time series values. It is characteristic of the appearance of a plateau.

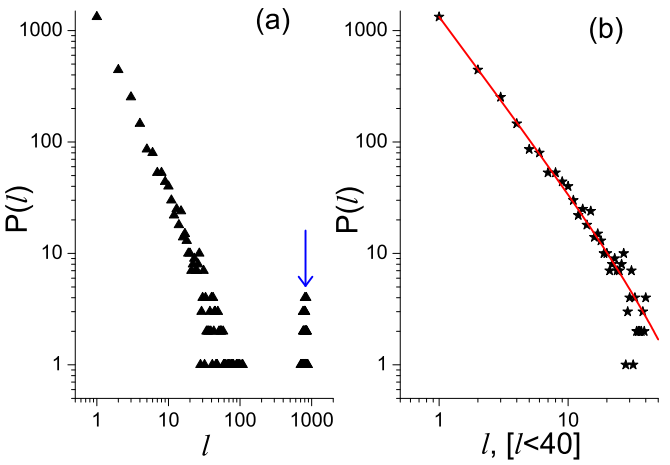

FIG. 7. (a) Distribution of waiting times. For very long waiting times ($700 < l < 900$) a very narrow distribution is observed as indicated by the arrow. (b) For waiting times $l < 40$ an excellent power law appears; the fitting line is given by the Eq. (2) with $p_2 = 1.55$, $p_3 = 0.01$, and $R^2 = 0.999$.

deviation) and then we calculate the distribution of $V_{bt}(t)$ [Fig. 6(b)]. We observe from Fig. 6(b) that the distribution of $V_{bt}(t)$ shows a flat maximum. Such a behavior is usually related to the presence of a marginally stable fixed point undergoing a tangent bifurcation [20]. Assuming that this scenario applies also in the present case, the plateau region is interpreted as the immediate neighborhood of the bifurcating fixed point [21,26]. To ensure that the plateau region is related to criticality we have to calculate the distribution of the corresponding waiting times. In our case the term "waiting times" denotes the number of successive time steps for which the $V_{bt}(t)$ trajectory stays within the plateau. As shown in [22], if the plateau region has a critical origin, the distribution of the corresponding waiting times follows the power law with an exponent $p_l > 1$. Furthermore, in [22], using the magnetization time series of the three-dimensional (3D) Ising model at the critical temperature, it has also been shown that the exponent p_l can be associated with the isothermal critical exponent δ through the relation $p_l = 1 + 1/\delta$ [20]. The plateau region is not strictly defined. To overcome this ambiguity we assume a variable width of the plateau and we check the robustness of our results with respect to small changes of the plateau width. Note that the plateau is mentioned as the "laminar region" in previous works of ours. Therefore, from this point on we will use the term "laminar region" to denote the plateau of $V_{bt}(t)$ distribution.

The next step in the application of MCF is the estimation of the distribution of the waiting times for varying the width of the laminar region. A reasonable estimation of the laminar region is within the interval $[-0.15,0.15]$ (maximum width of laminar region $= 0.3$) as can be seen in Fig. 6(b). The final step in the MCF is to use the function

$$P(l) = p_1 l^{-p_2} e^{-p_3 l} \tag{2}$$

to fit the experimentally determined waiting times distribution and calculate the corresponding parameters p_2, p_3. As shown in [22,23], this function takes care of two important issues: (i) the finite size effects, and (ii) the distance from the critical point. Both are simulated by the presence of the exponential factor $e^{-p_3 l}$ in Eq. (2). This term is a crucial indicator of the proximity to the critical point (critical frequency in our case), if any, since it dominates far away from criticality while it becomes zero as we approach the critical frequency. When $p_3 = 0$ then the exponent p_2 in Eq. (2) should coincide with the above mentioned critical exponent p_l. An indicative estimation of the distribution of the waiting times for the laminar region [0,0.15] is presented in Fig. 7.

From the results obtained after the application of MCF a very interesting conclusion is reached. There are two components in the $V_{bt}(t)$ time series. In terms of waiting times distribution, these components are separated by a "depletion" zone characterized by the absence of any waiting times. One component is a "noisy," unstructured background without any dynamics corresponding to the very long waiting times [indicated by the arrow in Fig. 7(a)] and the other component, for $l < 40$ [cf. Fig. 7(b)], presents fluctuations induced by intermittent dynamics since the waiting times follow a power-law distribution. It is obvious that without the MCF analysis the second component would be well hidden.

By restricting our study of the 5 kHz $V_{bt}(t)$ time series to the low waiting times ($l < 40$) and repeating the previous procedure for different laminar regions (different widths of the laminar region), the results shown in Fig. 8 were obtained. Figure 8 portrays the exponents p_2, p_3 vs the width of the laminar region. We observe that for a wide range of laminar region widths, where almost all $V_{bt}(t)$ values belonging to the plateau of the amplitude distribution shown in Fig. 6(b) are included, the calculated exponent pairs (p_2, p_3) take values satisfying conditions implied by thermal critical systems, namely, $p_2 > 1$ and $p_3 \approx 0$. The closer to zero is the value of p_3, the closer to pure power law is the distribution of waiting times according to the model of Eq. (2). As can be verified from Fig. 8, a "competitive," anticorrelated relation exists between the two exponents. Indeed, when the exponent p_3 takes the lower value (see blue downward arrow in Fig. 8), i.e., closer to pure power law, the exponent p_2 takes its maximum value (see green upward arrow in Fig. 8) and vice versa.

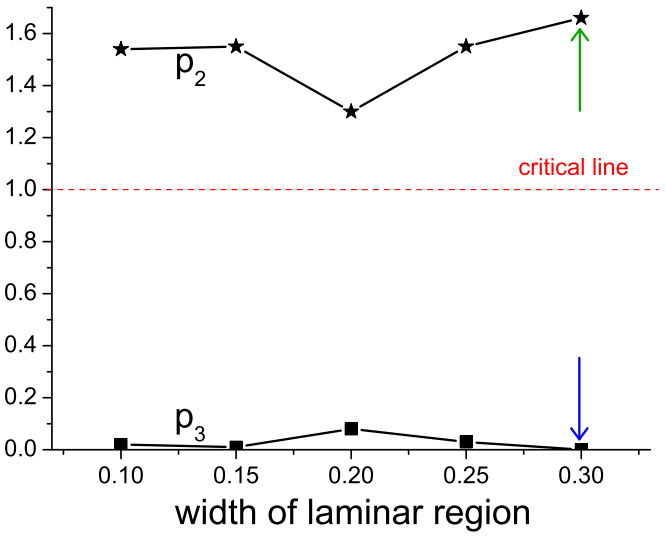

FIG. 8. The fitting exponents p_2, p_3 vs the width of the laminar region for the 5 kHz $V_{bt}(t)$ time series.

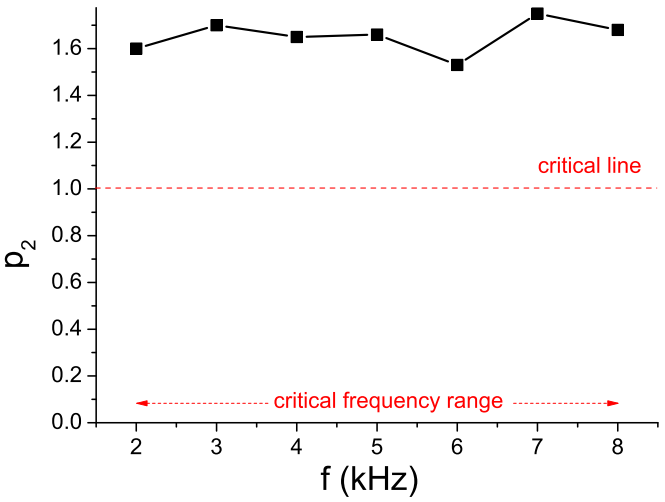

FIG. 10. The maximum p_2 exponent value vs frequency within the critical band.

A key characteristic of phase transition is the critical point which separates the two phases. In a typical critical system, according to the Ginzburg criterion [27,28], there is a zone around the critical point where the order parameter fluctuations possess scaling properties.

Although criticality has been revealed for 5 kHz, according to the Ginzburg criterion, we would expect the occurrence of critical behavior in a frequency band near the transition point and not just at a single critical frequency. In order to determine the range of the expected "Ginzburg zone" (critical frequencies band), we repeat the application of MCF on all the frequencies from 2 to 20 kHz [above which the quality of fitting to the model of Eq. (1) is destroyed]. From plots like that of Fig. 8 we find the minimum values of p_3 (see downward blue vertical arrow) for each frequency, which are depicted in Fig. 9. Note that, as already noted, these cases are closer to pure power law. It can be concluded from Fig. 9 that there is a frequency band,

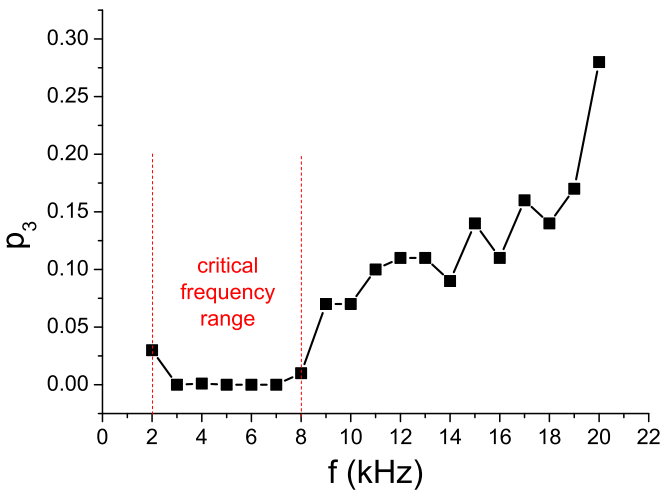

FIG. 9. The minimum p_3 exponent vs frequency. Within a narrow zone from 2 to 8 kHz the minimum p_3 values are very close to zero, indicating critical dynamics.

from 2 to 8 kHz, where the minimum values of p_3 are very close to zero. Therefore this zone of frequencies could be considered as the critical Ginzburg zone presenting the characteristics of the critical point of a second-order phase transition between phase A and phase B. Within the specific zone, the fluctuations of V_{bt} (or equivalently of V_R) demonstrate dynamics similar to the intermittent dynamics of the order parameter in a thermal critical state [21]. As the frequency departs from the critical zone the distribution $P(l)$ attains a dominating exponential tail. Note that the revealed Ginzburg zone is rather narrow, as compared with the very long separation frequency distance between the two discrete phases A and B.

As can be seen from Fig. 8, the exponent p_2 values obtained for a specific frequency and variable laminar region widths, although all satisfying the critical condition $p_2 > 1$, are characterized by a strong fluctuation. Therefore, the estimation of a characteristic value of power-law exponent p_l, such that $P(l) \sim l^{-p_l}$, which would allow us to estimate the corresponding isothermal critical exponent δ through $p_l = 1 + 1/\delta [= 1 + 1/(z-1)]$ [20], is not possible. However, for a specific frequency, we could use the value of the exponent p_2 corresponding to the minimum value of exponent p_3 as a representative value, since for this case the distribution of waiting times is closer to a pure power law and therefore closer to criticality. Clearly, this is the maximum p_2 value obtained for a specific frequency (for example, for the case of 5 kHz, see the upward green vertical arrow in Fig. 8). Figure 10 shows these maximum exponent p_2 values for the critical frequency band, namely, for frequencies from 2 to 8 kHz.

As shown in Fig. 10, the fluctuation of the p_2 exponent is limited, rendering the calculation of a mean value meaningful. The calculated mean p_2 exponent over the critical frequency zone was found to be $\langle p_2 \rangle = 1.65$. Since the approximation $p_l = p_2$ is valid in the critical state, we obtain the estimation of a characteristic p_l value, $p_l = \langle p_2 \rangle = 1.65$, leading to $\delta = 1.5$. This value of δ does not correspond to any known universality class in the context of thermal systems. This is expected since the observed transition being driven by

frequency tuning could merely be related to a dynamical (or structural) process.

V. FRACTAL ANALYSIS

Different methods for the estimation of the Hurst exponent, as an expression of the roughness of a time series, or the long-term memory (long-term persistence) of the associated complex process, are usually applied in cases of time series characterized by certain scaling (fractal) characteristics. Some of the most widely used methods are the direct estimation of the Hurst exponent H by means of the rescale range (R/S) analysis; the estimation of the scaling exponent β, of the power spectral density (PSD); and detrended fluctuation analysis (DFA), through the estimation of the corresponding scaling exponent a. Note that the DFA exponent a is related to the Hurst exponent H [29,30], and the spectral power-law exponent β [31]. Specifically, in the case of a fractional Brownian motion (fBm) time series it is [32,33] $H = a-1$ and $\beta = 2a-1$.

We examine here the V_{bt} time series in terms of R/S analysis in order to have a direct estimation of H, as well as using DFA because it presents an advantage over spectral analysis and R/S analysis in detecting long-range correlations embedded in a seemingly nonstationary time series, and also avoids the spurious detection of apparent long-range correlations that are an artifact of nonstationarity [34]. It is noted that other methods for the estimation of the Hurst exponent have also been proposed, such as the moving averages crossings method which is reported to provide calculation accuracy of the same order than the one of the DFA [35,36]. Although methods based on PSD scaling are known for being commonly superior to DFA in terms of bias and variance of the estimated Hurst exponents [37] we do not proceed to such an analysis here for brevity reasons.

In the following we briefly provide key information and formulas regarding the R/S and the DFA methods, in Secs. V A and V B, respectively, while the results obtained after the analysis of the V_{bt} time series in terms of these two methods are presented in Sec. V C.

A. Rescale range analysis

The rescale range (R/S) analysis was originally introduced for the analysis of hydrological data [29,30]. It is based on two quantities: first, the range R_n, which is the difference between the maximum and minimum values of the accumulated departure of the time series from the mean, calculated over each one $(n = 1, 2, \ldots, d)$ of the m-samples-long subseries in which the time series can be divided; and second, the standard deviation of the corresponding subseries S_n. The so-called rescaled range is exactly the ratio of R to S. Hurst [29] found that (R/S) scales by power law as time (i.e., the sample length m of the subseries) increases,

$$(R/S)_m \propto m^H, \tag{3}$$

where H is the Hurst exponent, an empirical relation well describing a variety of time series of natural phenomena. The exponent H is estimated as the linear slope of a $\log(R/S)_m - \log m$ representation.

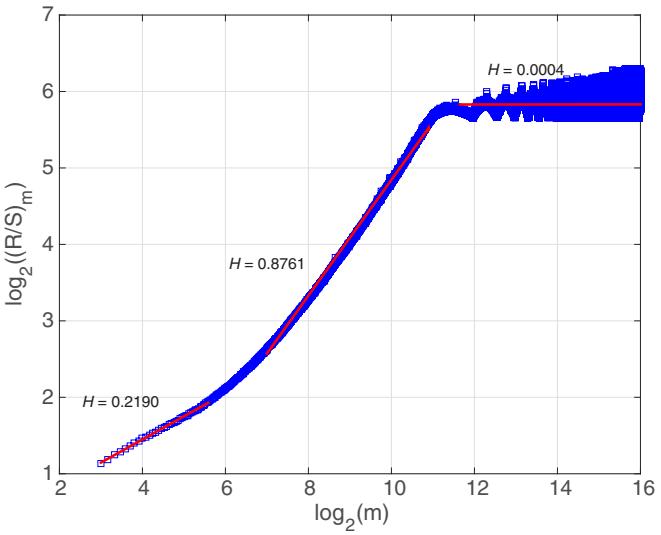

FIG. 11. Three segments piecewise linear approximation of the $\log(R/S)_m - \log m$ representation. The slopes, attributed to "local" Hurst exponents over the three scale ranges, are shown.

B. Detrended fluctuation analysis

Detrended fluctuation analysis (DFA) is a straightforward technique for identifying the extent of fractal self-similarity in a seemingly nonstationary time series [34,38]. After dividing a time series to subseries of m-samples length, the root mean-square fluctuation for the integrated and detrended series, $F(m)$, is calculated. Repeating this calculation for different m, a power-law relation between $F(m)$ and time (expressed by subseries length m),

$$F(m) \propto m^a, \tag{4}$$

indicates the presence of scaling. The DFA exponent a is estimated as the linear slope of a $\log F(m) - \log m$ representation.

C. Fractal analysis results

The analysis of the full length of the 5 kHz $V_{bt}(t)$ critical signal in terms of R/S analysis and DFA yielded the results portrayed in Figs. 11 and 12, respectively. It is noted that a time series corresponding to 100 periods of the $V_{bt}(t)$ signal sampled at $f_s = 20\,\text{MHz}$, i.e., with a sampling period of $T_s = 50\,\text{ns}$, and corresponding to a total length of 10 ms was analyzed. As can be clearly seen from these figures, there is no typical scale-invariant, (mono)fractal behavior over the whole time-scale range. However, the full range of time scales could be roughly divided into three different ranges of scales approximated by linear slopes:

The first slope is identified for time scales less than $\sim 3.2-6.4\,\mu\text{s}$, yielding a Hurst exponent $H = 0.22$ (Fig. 11). This result indicates antipersistent behavior, implying that fluctuations tend to induce stability within the system as in a negative feedback process. Note that this scale range corresponds to the high-frequency variations within one period of the analyzed signal [cf. Fig. 4 for an indicative period of $V_{bt}(t)$ for 5 kHz driving frequency]. On the other hand, DFA analysis at the same range of time scales reveals a steep increase of the fluctuation function with a slope of $a = 1.70$

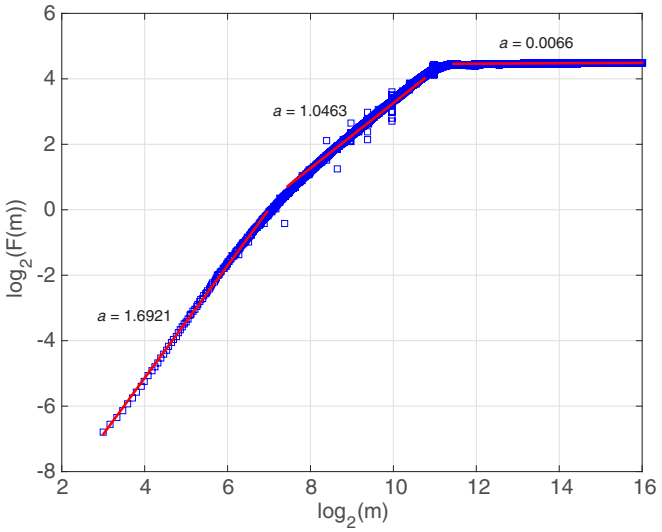

FIG. 12. Three segments piecewise linear approximation of the $\log F(m) - \log m$ representation. The slopes, attributed to "local" a exponents over the three scale ranges, are shown.

(Fig. 12) indicating a quite smooth time series, which is in agreement with the information retrieved through the R/S analysis.

The second slope is identified in the middle time scales, from $\sim 3.2-6.4\,\mu$s up to 0.1 ms, corresponding to $H = 0.88$ (Fig. 11) and $a \approx 1$ (Fig. 12), which could be interpreted as near-pink $(1/f)$ noise. However, one should not overlook the fact that the specific range of time scales is dominated by the apparent periodicity imposed by the driving signal and the preprocessing for obtaining $V_{bt}(t)$ from the originally measured $V_R(t)$ time series. Note also that the abrupt changes resulting from the way the $V_{bt}(t)$ time series was constructed is probably a reason for the observed increased Hurst exponent estimates. It is noted that this interpretation is compatible with the view that the presence of different slopes (crossovers) in the scaling behavior should be carefully evaluated. As has been reported [39,40], this might not be a result of the existence of different scaling regions with different correlation properties but could be a result of the existence of trends or nonstationarities in the analyzed time series.

The third region, for time scales longer than 0.1ms, gives $H \approx 0$ and $a \approx 0$, revealing the scale-invariance boundary at the upper scales (low frequency) due to finite size effect.

The first (lower time scales) range seems to be the most reliable in terms of fractal analysis; therefore we focus on it. Moreover, this is the most interesting time-scale range, since, in terms of the MCF analysis, high-frequency variations correspond to the short waiting times ($l < 40$) for which intermittent criticality was revealed. The R/S analysis and DFA results for the lower scales imply a smooth, antipersistent, long-range dependence behavior which is in full agreement with the revealed second-order phase transition, for which the transition from one phase to the other is taking place smoothly without abrupt changes. Fractal analysis is also in agreement with the MCF analysis concerning the conclusion that there is no point in including the long time scales in the study. For scales longer than 0.1ms, i.e., for durations longer than one period of the $V_{bt}(t)$ for the 5-kHz driving frequency, no scale-invariance information is found. This is compatible with the MCF conclusion that for very long waiting times no structure is detected. The only reason one needs to include more than one period of the $V_{bt}(t)$ signal in the analysis is to achieve reliable statistics for the high-frequency fluctuations happening during the reverse-recovery effect and thus obtain more reliable results for the short waiting times (and short time-scales) analysis.

Interestingly, for the used 1N4004 rectifier diode with a typical zero-bias junction capacitance $C_j \sim 15$ pF, a maximum reverse-recovery time of the order of $1-10\,\mu$s is expected (a $\tau_{RR} \sim 700$ ns has been measured at 20 kHz for a diode of similar characteristics, 1N4007 [14], while different vendors specify, under a variety of different measuring conditions, maximum or typical reverse-recovery times in the range $1-30\,\mu$s). These might be considered as indicative maximum time scales for the studied RLD circuit, verifying the significance of the lower time-scale range revealed by fractal analysis in the observed nonlinear dynamic behavior. Note that 1N4004 is commonly given as a replacement of the 1N1221 diode appearing in relevant past publications.

VI. DISCUSSION AND CONCLUSION

The transition from low to high frequencies in a nonautonomous RLD circuit was found to present common characteristics with a thermal system undergoing a second-order phase transition. Using the method of critical fluctuations (MCF) we found a critical zone of frequencies in which the fluctuations of the voltage drop across the resistor of an RLD circuit, or equivalently the directly proportional current through the circuit, possess an intermittent component similar to the dynamics of the order parameter fluctuations of a thermal critical system. Specifically, intermittency-induced criticality was revealed signifying a second-order phase transition between the normal rectifier phase in the low frequencies and a full-wave conducting, capacitorlike phase in the high frequencies. The scaling exponent was estimated to be $p_l = 1.65$.

In order to interpret the observed behavior we suggest the following scenario: Within the critical frequency band, namely, between 2 and 8 kHz, the minority carriers form critical clusters, each one characterized by a different reverse-recovery time, τ_{RR}, leading to a reverse current which is expressed by the dynamical fluctuations of the voltage V_{bt}. As is known [41], the geometry of critical clusters is fractal. Therefore, we expect that at the critical zone of frequencies, the minority carriers get organized in self-similar clusters with fractal formations in the 3D space. Notably, a fractal analysis of the studied critical time series, by means of rescale-range (R/S) and detrended fluctuation analysis (DFA), revealed that V_{bt} variations present scale-invariance characteristics fully compatible with the findings of the corresponding critical dynamics analysis.

In analogy to a thermal system undergoing a second-order transition such as, for example, the Ising model in $D \geqslant 2$ dimensions, phase B corresponds to the symmetric phase, while phase A corresponds to the phase of spontaneously broken symmetry; the driving frequency resembles the role

of the temperature as the control parameter. In order to describe the transition within the theoretical framework of critical phenomena the introduction of an order parameter is necessary. Typically, in a thermal phase transition the mean magnetization plays the role of such a quantity where during the symmetric phase the mean value of the order parameter is zero, while in the broken phase it is nonzero. In the case of the considered circuit (cf. Sec. II, Fig. 1), we observe that the change of normalized turning points density vs frequency f, as shown in Fig. 5, becomes almost zero for near-sinusoidal, normal conducting $V_R(t)$ (high frequencies), while it takes a nonvanishing finite, almost constant value in the rectifying regime at low frequencies ($f < 1$ kHz). Thus it possesses the basic characteristics of an order parameter.

The presented analysis introduces an alternative insight to the dynamics of the hole-electron pairs in a *p-n* junction diode. Nevertheless, more effort is required in order to better understand the observed phase transition at both the theoretical and experimental levels. The comprehension of such phenomena often calls for long and extensive research, as in the case of the Branly phenomenon [42,43].

ACKNOWLEDGMENTS

The authors would like to express gratitude to Professor C. Nomicos for providing the digital oscilloscope used during the experiments of this study.

[1] P. S. Linsay, Phys. Rev. Lett. **47**, 1349 (1981).
[2] J. Testa, J. Perez, and C. Jeffries, Phys. Rev. Lett. **48**, 714 (1982).
[3] E. Hunt, Phys. Rev. Lett. **49**, 1054 (1982).
[4] C. Jeffries and J. Perez, Phys. Rev. A **26**, 2117 (1982).
[5] R. W. Rollins and E. R. Hunt, Phys. Rev. Lett. **49**, 1295 (1982).
[6] L. O. Chua, M. Hasler, J. Neirynck, and P. Verburgh, IEEE Trans. Circuits Syst. **29**, 535 (1982).
[7] A. Azzouz, R. Duhr, and M. Hasler, IEEE Trans. Circuits Syst. **30**, 913 (1983).
[8] R. W. Rollins and E. R. Hunt, Phys. Rev. A **29**, 3327 (1984).
[9] A. Azzouz, R. Duhr, and M. Hasler, IEEE Trans. Circuits Syst. **31**, 587 (1984).
[10] Z. Su, R. W. Rollins, and E. R. Hunt, Phys. Rev. A **40**, 2689 (1989).
[11] A. Azzouz and M. Hasler, IEEE Trans. Circuits Syst. **37**, 1330 (1990).
[12] T. L. Carroll and L. M. Pecora, Phys. Rev. E **66**, 046219 (2002).
[13] Hugo L. D. de S. Cavalcante and J. R. Rios Leite, Phys. Rev. E **66**, 026210 (2002).
[14] R. Mariz de Moraes and S. M. Anlage, Phys. Rev. E **68**, 026201 (2003).
[15] M. P. Hanias, G. Giannaris, A. Spyridakis, and A. Rigas, Chaos, Solitons Fractals **27**, 569 (2006).
[16] M. P. Hanias, Z. Avgerinos, and G. S. Tombras, Chaos, Solitons Fractals **40**, 1050 (2009).
[17] J. A. Kalomiros, S. G. Stavrinides, A. N. Miliou, I. P. Antoniades, L. Magafas, and A. N. Anagnostopoulos, Nonlinear Anal: Real World Appl. **10**, 691 (2009).
[18] Y. Ono, K. Fukushima, and T. Yazaki, Phys. Rev. E **52**, 4520 (1995).
[19] K. Fukushima and T. Yamada, J. Phys. Soc. Jpn. **57**, 4055 (1988).
[20] H. G. Schuster, *Deterministic Chaos: An Introduction* (Wiley-VCH, Weinheim, 1988).
[21] Y. F. Contoyiannis and F. K. Diakonos, Phys. Lett. A **268**, 286 (2000).
[22] Y. F. Contoyiannis, F. K. Diakonos, and A. Malakis, Phys. Rev. Lett. **89**, 035701 (2002).
[23] Y. F. Contoyiannis, F. K. Diakonos, C. Papaefthimiou, and G. Theophilidis, Phys. Rev. Lett. **93**, 098101 (2004).
[24] Y. F. Contoyiannis, P. G. Kapiris, and K. A. Eftaxias, Phys. Rev. E **71**, 066123 (2005).
[25] Y. F. Contoyiannis and F. K. Diakonos, Phys. Rev. E **76**, 031138 (2007).
[26] F. K. Diakonos and P. Schmelcher, Chaos **7**, 239 (1997).
[27] A. P. Levanyuk, Zh. Eksp. Teor. Fiz. **36**, 810 (1959) [Sov. Phys. JETP **9**, 571 (1959)].
[28] V. L. Ginzburg, Fiz. Tverd. Tela **2**, 2031 (1960) [Sov. Phys. Solid State **2**, 1824 (1961)].
[29] H. Hurst, Trans. Am. Soc. Civ. Eng. **116**, 770 (1951).
[30] B. B. Mandelbrot and J. R. Wallis, Water Resour. Res. **4**, 909 (1968).
[31] C. Heneghan and G. McDarby, Phys. Rev. E **62**, 6103 (2000).
[32] S. V. Buldyrev, A. L. Goldberger, S. Havlin, R. N. Mantegna, M. E. Matsa, C.-K. Peng, M. Simons, and H. E. Stanley, Phys. Rev. E **51**, 5084 (1995).
[33] S. Shadkhoo, F. Ghanbarnejad, G. R. Jafari, and M. R. R. Tabar, Cent. Eur. J. Phys. **7**, 620 (2009).
[34] C.-K. Peng, S. Havlin, H. E. Stanley, and A. L. Goldberger, Chaos **5**, 82 (1995).
[35] N. Vandewalle and M. Ausloos, Phys. Rev. E **58**, 6832 (1998).
[36] N. Vandewalle, M. Ausloos, and Ph. Boveroux, Physica A **269**, 170 (1999).
[37] A. Witt and B. D. Malamud, Surv. Geophys. **34**, 541 (2013).
[38] C.-K. Peng, S. V. Buldyrev, S. Havlin, M. Simons, H. E. Stanley, and A. L. Goldberger, Phys. Rev. E **49**, 1685 (1994).
[39] K. Hu, P. Ch. Ivanov, Z. Chen, P. Carpena, and H. E. Stanley, Phys. Rev. E **64**, 011114 (2001).
[40] Z. Chen, P. Ch. Ivanov, K. Hu, and H. E. Stanley, Phys. Rev. E **65**, 041107 (2002).
[41] N. G. Antoniou, Y. F. Contoyiannis, F. K. Diakonos, and C. G. Papadopoulos, Phys. Rev. Lett. **81**, 4289 (1998).
[42] S. Dorbolo, M. Ausloos, and N. Vandewalle, Phys. Rev. E **67**, 040302(R) (2003).
[43] S. Dorbolo, M. Ausloos, N. Vandewalle, and M. Houssa, J. Appl. Phys. **94**, 7835 (2003).